Discovery of zerumbone as a new agent for cardiac hypertrophy by high-throughput screening using human embryonic stem cell-derived cardiomyocytes

Jie Huang
Fudan University
Haiyan Chen
Zhongshan Hospital/Fudan University
Shujue Lan
Shanghai Institute of Biochemistry and Cell Biology/Chinese Academy of Sciences
Le Qin
Fudan University
Zixuan Xun
Fudan University
Shuai Han
Shanghai Institute of Biochemistry and Cell Biology/Chinese Academy of Sciences
Hongwei Zhao
Shanghai Institute of Biochemistry and Cell Biology/Chinese Academy of Sciences
Yunqing Ci
Shanghai Institute of Biochemistry and Cell Biology/Chinese Academy of Sciences
Chen Xu
Fudan University https://orcid.org/0000-0001-5146-5260
Wenjia Zhu
Fudan University
Xinya Lu
Fudan University
Jiaxin Chen
Fudan University
Qiuyi zheng
Fudan University
Ermin Li
Northwestern University https://orcid.org/0000-0002-0301-4155
Xinyun Chen
Shenzhen University

Chao Lu
Fudan University https://orcid.org/0000-0002-9484-6415
Ruizhe Qian
Fudan University
Sifeng Chen
Fudan University
Xiaobo Li
School of Basic Medical Sciences, Fudan University https://orcid.org/0000-0001-7737-1721
Ning Sun (sunning@fudan.edu.cn)
Jiangnan University https://orcid.org/0000-0002-7861-3646

Article

Keywords:

Posted Date: April 13th, 2022

DOI: https://doi.org/10.21203/rs.3.rs-574349/v1

Abstract

Background: Pathological cardiac hypertrophy is considered an adaptive response of the heart due to cardiovascular diseases such as hypertension, aortic and valvular stenosis, and inherited cardiomyopathy caused by mutations in sarcomeric proteins. It is a risk factor of various forms of cardiovascular diseases and closely associated with heart failure. Current medications for cardiac hypertrophy are limited and often only target the symptoms without a radical effect. There is a strong demand for developing new drugs to improve the overall treatment.

Methods: We firstly established a hypertrophy model of human embryonic stem cell (hESC)-derived cardiomyocytes by norepinephrine treatment. Using high-throughput drug screening a library of small-molecule natural products and high-content analyses of hESC-cardiomyocyte size, we identified zerumbone as an effective new agent alleviating concentric cardiac hypertrophy. The downstream molecular pathway induced by zerumbone was identified by RNA-seq analyses of zerumbone treated hESC-cardiomyocytes and confirmed by biochemical studies.

Results: We found that zerumbone not only inhibited norepinephrine-induced hypertrophy of hESC-derived human cardiomyocytes *in vitro*, but also alleviated cardiac hypertrophy in spontaneous hypertensive rats and Mybpc3-G790A hypertrophic cardiomyopathy mice *in vivo*. This inhibition of cardiac hypertrophy by zerumbone was not dependent on lowering blood pressure. We further found that zerumbone markedly activated the NRF2/HO-1 related signaling pathway which showed a cardioprotective effect on cardiac hypertrophy. Zerumbone directly bound to and induced high molecular weight KEAP1, which impeded the interaction of CUL3 with KEAP1, leading to the inhibition of NRF2 ubiquitination and NRF2 accumulation and translocation into the nucleus. Inhibition of HO-1 expression blocked the effect of zerumbone in attenuating cardiomyocyte hypertrophy.

Conclusion: Our data indicate that zerumbone is an effective small molecule alleviating pathological cardiac hypertrophy. It could be used in combination with current antihypertensive drugs for hypertension patients with cardiac hypertrophy and may also be used for patients of inherited hypertrophic cardiomyopathy.

Introduction

Cardiac hypertrophy, including physiological and pathological hypertrophy, is an adaptive response of the heart to cardiac stress. Not like physiological hypertrophy that maintains cardiac function overtime without interstitial fibrosis and cell death, pathological hypertrophy accompanies continued adverse cardiac remodeling and leads to heart failure, arrythmia, and sudden death. Concentric cardiac hypertrophy is one form of the pathological hypertrophy characterized by increased cardiac muscle mass, thickened ventricular wall and septum, and reduced ventricular chamber. Pathological concentric cardiac hypertrophy is often caused by pressure overload, such as hypertension and aortic/valvular stenosis, and by mutations in sarcomeric proteins as inherited hypertrophic cardiomyopathy (HCM). Hypertension

becomes a worldwide pandemic disease and a large fraction of hypertension patients develop left ventricular hypertrophy(*1*), while HCM also has a non-trivial incidence of ~1:500 in adult humans(*2*).

Inhibiting ventricular hypertrophy has been shown to be beneficial and considered as an attractive therapeutic strategy for cardiac hypertrophy patients(*3*). Current medications for cardiac hypertrophy, such as β-blockers, calcium antagonists, angiotensin-converting enzyme inhibitors, and other medicines, commonly target the symptoms to partially improve cardiac systolic and diastolic function, without a radical effect for the disease(*4, 5*). These medications have a ceiling effect and only bring about 10%-20% regression of left ventricular mass, and even regression, in cardiac hypertrophy patients(*6*). It remains a strong demand for developing new drugs and treatments for cardiac hypertrophy.

With the advancement of pluripotent stem cells and cardiac-specific differentiation techniques, it is now possible to derive large scale pure human cardiomyocytes (CMs) for high-throughput drug screening and toxicity test(*7-9*). In this study, we established a norepinephrine (NE)-induced *in vitro* hypertrophy model of human embryonic stem cell derived CMs (hESC-CMs) and used it for high-throughput screening of a library containing 495 small-molecule natural products. Through high-content analyses of cell size and two rounds of high-throughput screening, we identified 19 small-molecule natural products that can inhibit the NE-induced hypertrophy in hESC-CMs. Using the *in vivo* cardiac hypertrophy model of spontaneous hypertensive rats (SHRs), we narrowed down to zerumbone, a cyclic eleven-membered sesquiterpene isolated from the tropical plant *Zingiber zerumbet*, as an effective agent for pressure overload-induced hypertrophy in *vivo*. This inhibition of cardiac hypertrophy by zerumbone was not dependent on lowering blood pressure. We further evaluated the anti-hypertrophy effect of zerumbone in HCM using the Mybpc3-G790A HCM mice and it showed that zerumbone inhibited the pathological hypertrophy and adverse cardiac remodeling in HCM. Using RNA-seq analyses of zerumbone treated hESC-CMs, we found that zerumbone specifically activated NRF2/HO-1 related signaling pathway shown to suppress cardiac maladaptation and hypertrophy(*10, 11*). We further found that zerumbone activated the NRF2 pathway through directly binding to KEAP1 and induced high molecular weight (HMW) KEAP1. This impeded the interaction between CUL3 and KEAP1, leading to the inhibition of NRF2 ubiquitination. NRF2 accumulation and translocation into the nucleus markedly activated HO-1 expression. Moreover, this anti-hypertrophy effect of zerumbone can be specifically blocked by a HO-1 inhibitor *in vitro*.

Overall, by high-throughput drug screening and high-content analyses, we found that zerumbone is an effective small molecule alleviating pathological cardiac hypertrophy both in pressure-overload model of SHR and in mutation-induced Mybpc3-G790A HCM mice. Our data showed that inhibition of hypertrophy by zerumbone was not dependent on blood pressure lowering. Zerumbone could be used in combination with current antihypertensive drugs for hypertension patients manifesting cardiac hypertrophy and could also be used in treatments for patients of inherited hypertrophic cardiomyopathy in the future.

Results

Establish the high-throughput drug screening conditions using NE-induced hypertrophy of hESC-CMs

We previously established an H7 hESC line carrying a neomycin selection cassette after the last exon of MYL2 gene (cardiac myosin light chain-2v) and named this cell line as $MYL2^{Neo/WT}$-H7(*12*). By G418 selection after cardiac-specific differentiation of this cell line, we were able to constantly obtain >98% pure hESC-derived ventricular-like CMs (Fig. 1A and Supplementary Fig. 1). To establish a high-throughput drug screening system for cardiac hypertrophy, we seeded hESC-CMs in the 384-well plates and used NE to induce cardiomyocyte hypertrophy in *vitro*. For CMs recognition in microscopic images by high-content analysis, we first located nuclei with DAPI, and identified the positive CMs population with cTnT-staining. Owing to the incomplete coverage of the whole cytoplasmic area by myofilament staining, we chose Cell Tracker, a dye for cytoplasm, to calculate total cell area (Fig. 1B).

NE treatment of hESC-CMs increased the average cellular area, reduced the ratio of small CMs (1000-4000 mm^2), and enhanced the ratio of large CMs (4000-10000 mm^2) (Fig. 1D, Supplementary Fig. 2A). After testing different NE concentrations and treating time, we found that 5 days treatment of 20 mM NE resulted in the optimal separation between the control- and NE-treated groups in cell size, ratio of small CMs, and ratio of large CMs with a coefficient of variation (CV) under 25% by high-content imaging analyses (Supplementary Fig. 2A-2B, Supplementary Table 1). We further tested this condition using the a-blocker prazosin. 20 mM prazosin treatment significantly reduced the average cell area and the ratio of large CMs, proving the hESC-CMs well responded to drugs inhibiting NE (Supplementary Fig. 3A-3D). We then used the condition of 20 mM NE and 5 days treatment in our subsequent high-throughput screening studies.

Identification of Zerumbone through high-throughput screening for 495 natural small molecules in purified hESC-CMs

After developed the high content screen with an immunofluorescent cell-based assay in a 384-well format through an automated staining protocol and image microscopy system, we screened a library containing 495 small-molecule natural compounds isolated from natural products. All compounds were screened in 4 duplicated wells at 10 μM. We identified 54 positive hits after primary screen and 19 positive hits after secondary screen (Fig. 1C). Through evaluation of subsequent dose dependent assays, cytotoxicity assays, CMs functional assays, as well as commercial availability, a compound, zerumbone (Hit-3), emerged from these 19 hits (Fig. 1C, Supplementary table 2). The other listed top 4 hits (Hit-1, 2, 4, 5) are still under further investigation in our lab. Here we only provided partial data of these hits which showed an inhibition on the beating frequency and contraction force of NE-treated hESC-CMs (Supplementary Fig. 3A-3B). Among these 19 hits, Hit-10 (9-cis-Retinoic acid) and Hit-11 (13-cis-Retinoic acid) were different conformers which have been reported to inhibit the expression of cardiac hypertrophy-related marker genes(*13*). Hit-14 (Ursolic acid) has also been reported to improve cardiac hypertrophy and fibrosis(*14-16*). It was worth noting that we found Hit-6 (Rauwolscine) was an antagonist of α adrenoreceptor, which was similar to prazosin that used as the positive control in our study(*17*). To some extent, this result (Hit-6) reflected the reliability of our screening system. Considering the novelty of our research, we halted further study of these hits that have been reported to inhibit cardiac hypertrophy. Due to commercial availability in China, Hit-13 (Forskolin) and Hit-15 (Ingenol 3,20-

dibenzoate) were not conveniently obtained and not extensively studied. Hit-16 to 19 (13-O-Acetylphorbol, Phorbol 12,13-dibutyrate, Phorbol 12-myristate 13-acetate, and 12-Deoxyphorbol 13-phenylacetate 20-acetate) were all phorbol with highly toxicity(*18, 19*) and not chosen for further studies. Hit-8 (Cepharanthine) exhibited significant inhibition of beating rates in hESC-CMs without a dose-dependent anti-NE effect (Supplementary Figure 3A). Hit-7 (Emodin) and Hit-8 both showed significant negative influence on the morphology of cardiomyocytes (Supplementary Fig. 3C-3E). These two compounds with seemingly high toxicity were also not chosen for further study. Hit-7, 9 (Geranylgeranoic acid) and 12 (7-Hydroxyflavone) did not show a significant inhibitory effect of NE-induced increase of beating rates in cardiomyocytes (Supplementary Fig. 3A) and were not further studied as well. Here, we present all the data of zerumbone (Hit-3) in this study.

Zerumbone showed a dose-dependent anti-NE effect (IC_{50}=16.70 ±2.659 μM) on beating rates in hESC-CMs (Fig. 1E). Cytotoxicity assay showed that zerumbone had a low toxicity to CMs viability with an IC_{50}=58.65 μM (Fig. 1F), which was far lower than the screening concentration (10 μM). This indicated that under the screening condition, CMs were still in a relatively high viability state, and the recovery of cell area was not due to inhibition of the cell viability. Collectively, high-content screening for small molecules in purified hESC-CMs and profiling assays led to the identification of zerumbone as a potential candidate for inhibiting CMs hypertrophy.

Zerumbone prevents the hypertrophy phenotype of hESC-CMs induced by NE

Next, we assessed the effect of zerumbone on NE-induced cardiac hypertrophy in hESC-CMs. NE treatment led to an increase in CMs cell area and upregulation of the hypertrophy markers B-type natriuretic peptide (*BNP*) and atrial natriuretic peptide (*ANP*) (Fig. 2A-2C). Expression of the structural and contractile related genes, such as cardiac troponin T (*TNNT2*), myocyte-specific enhancer factor 2C (*MEF2C*) and sarcoplasmic reticulum Ca^{2+}-ATPase 2a (*SERCA2a*) were also significantly upregulated (Supplementary Fig. 4E). Pretreatment with zerumbone inhibited NE-induced enlargement of CM size and up-regulation of these genes (Fig. 2A-2C, Supplementary Fig. 4E).

In CMs functional assays, we found that NE showed a positive inotropic effect on CMs with enhanced contraction and faster beating frequency after treatment (Fig. 2D-2F). The contraction force and beating rates were decreased with zerumbone or prazosin treatment, which indicated that zerumbone could inhibit the effect of NE on CMs contractility. Previous studies showed that Ca^{2+} was closely related to heart contraction and cardiac hypertrophy, accompanied with activated Ca^{2+} fluxes regulation(*20, 21*). Angiotensin II or catecholamine can both activate intracellular Ca^{2+} channels in cardiomyocytes, and further activate calmodulin kinase (CaMK) and NFAT signaling pathways, which is key for promoting pathological cardiac hypertrophy(*22*). To assess the Ca^{2+} handling properties of hESC-CMs, we conducted Ca^{2+} imaging of hESC-CMs after zerumbone treatment for 24h. Zerumbone prolonged calcium transient duration, including time to peak and decay time, and decreased the transient amplitude (Fig. 2G-2H). Zerumbone prevents the effect of NE on cardiomyocytes in calcium handling to a certain extent.

Together, these results demonstrate that zerumbone reduces NE-induced cardiac hypertrophy in cultured hESC-CMs.

Zerumbone attenuates pressure overload-induced cardiac hypertrophy and remodeling in SHRs

To test whether zerumbone can alleviate cardiac hypertrophy in *vivo*, we used a pressure overload-induced cardiac hypertrophy model (Spontaneously hypertensive rats□SHR). At first, a pre-experiment was conducted to confirm the development process of cardiac hypertrophy in SHRs and determine the administration time of zerumbone. The blood pressure of SHRs increased from 6 weeks after birth, while cardiac hypertrophy became obvious from 8 weeks and the significant difference stay stable after 12 weeks after birth (Supplementary Fig. 5). SHRs and WKYs were exposed to the feedstuff containing captopril or zerumbone for 3 months. As an inhibitor of angiotensin converting enzyme (ACE), captopril is widely used as a positive control to lower blood pressure in SHRs. Here, we added captopril or zerumbone into rat feedstuff at the ratio of 0.1% in cap-high group, 0.02% in cap-low group, 0.07% in zer-high group and 0.035% in zer-low group respectively. We assumed the standard daily feedstuff consumption of ~20 g/day for a rat to yield a total of 100 mg · kg^{-1}· d^{-1} captopril intake in cap-high group, 20 mg · kg^{-1}· d^{-1} in cap-low group, 70 mg · kg^{-1}· d^{-1} zerumbone intake in zer-high group, and 35 mg · kg^{-1}· d^{-1} in zer-low group. Male SHRs were treated with zerumbone or captopril through processed feedstuff at 6 weeks old when blood pressure started to elevate without obvious cardiac hypertrophy and fibrosis (Supplementary Fig. 6A). The records of daily food consumption and body weight showed no significant differences between the treated groups and control groups (Supplementary Fig. 7A), indicating the addition of drug powders did not influence daily diet of rats and ensuring the absorption of drugs. After 3 months, SHRs developed obvious hypertrophy, as evidenced by increased heart gross morphology and heart weight to body weight ratio (Supplementary Fig. 6B-6C). WGA-staining also showed an enlargement of cardiomyocytes cross-sectional area (Supplementary Fig. 6D). Remarkably, these cardiac hypertrophic features were attenuated both in zerumbone and captopril treated groups (Supplementary Fig. 6B-6D). Consistently, upregulation of fetal genes (*β-MHC*, *BNP* and *ANP*), cardiac structure and function related genes (*TNNT2*, *SERCA2a* and *MEF2C*) and fibrosis related genes (*COL1A1*) in SHRs were suppressed in zerumbone treated groups (Supplementary Fig. 6F-6H). The fibrosis of SHRs was also inhibited with zerumbone treatment (Supplementary Fig. 6E). Echocardiography analysis also showed a decrease in the thickness of interventricular septum (IVSd), left ventricular posterior wall (LVPWd), and left ventricular mass index (LVMI) from zerumbone treated groups compared to SHRs (Supplementary Fig. 6I-6J, Supplementary Table 3). However, unlike captopril showed an obvious decrease in blood pressure, the blood pressure was not changed after zerumbone treatment in SHRs (Supplementary Fig. 7B).

Meanwhile, we also tested zerumbone in male aged SHRs (14-week-old) that developed an obvious cardiac hypertrophy before treatment (Fig. 3A). Like our studies in young SHRs, zerumbone reduced heart size, heart weight to body weight ratio, as well as cardiomyocytes area with WGA staining (Fig. 3B-3D). The mRNA levels of hypertrophic genes, like *β-MHC*, *BNP*, *ANP*, *TNNT2* and *MEF2C* were also downregulated with zerumbone treatment (Fig. 3F-3G). The fibrosis of SHRs was inhibited by zerumbone, with decreased fibrosis area and downregulation of *COL3A1* (Fig. 3E, 3H). The indexes of cardiac

hypertrophy based on echocardiography were decreased in IVSd, LVPWd and LVMI, increased in Dd in zerumbone treated SHRs (Fig. 3I-3J, Supplementary Table 4). In addition, we also conducted administration of zerumbone in female aged SHRs (14-week-old). As shown in Supplementary Fig. 8 and Supplementary Table 5, zerumbone also exhibited an anti-hypertrophic effect in female SHRs similar in male SHRs.

High dose of captopril caused a significant therapeutic effect on SHRs and the cardiac hypertrophy morphology almost returned to a normal level as WKYs (Fig. 3, Supplementary Fig. 6, 8, Supplementary Table 3-5). The anti-hypertrophic effect of zerumbone on SHRs was similar to the low dose of captopril. Thus, we further assessed the anti-hypertrophic effect of a combinative administration of zerumbone and captopril in SHRs. The feedstuff both containing zerumbone (high dose-0.07%) and captopril (low dose-0.02%) were given both to SHRs at 6 weeks old (male) and 14 weeks old (male and female). High dose of zerumbone in combination with low dose of captopril treatment markedly improved cardiac hypertrophy and remodeling of SHRs, presenting a similar anti-hypertrophic effect as the high dose of captopril treatment (Fig. 3, Supplementary Fig. 6 and 8, Supplementary Table 3-5).

At the molecular level, a great quantity of genes (3297) were upregulated in SHRs versus WKYs, while 1271 genes were downregulated with zerumbone treatment (Supplementary Fig. 9A). PCA analysis showed a significant separation between WKYs, SHRs and zerumbone treated group after 3 months treatment (Supplementary Fig. 10B). With GSEA analysis, we found that the calcium and MAPK signaling pathway, which are closely related to cardiac hypertrophy, were both upregulated in SHRs but downregulated upon zerumbone treatment (Supplementary Fig. 9C). And, these results were consistent with the improvement of cardiac hypertrophy we previously observed in SHRs at 6 weeks old treated with zerumbone (Supplementary Fig. 6).

Taken together, these results demonstrated that zerumbone could attenuate pressure overload-induced cardiac hypertrophy and remodeling in SHRs. And, the combination of zerumbone and antihypertensive drugs, like captopril, showed a remarkable anti-hypertrophic effect in SHRs. Importantly, such co-treatment could lower the dosage of antihypertensive medicine but raised a similar treatment effect, suggesting a potential beneficial effect of zerumbone in reducing medicinal doses of anti-hypertensive drugs but maintaining treatment effect for cardiac hypertrophy.

Zerumbone represses cardiac hypertrophy in HCM mice

Next, we further sought to examine whether zerumbone could repress cardiac remodeling in other hypertrophic models in *vivo*. We used a classic Mybpc3 knock-in (KI) HCM mouse carrying a point mutation (single G790A transition) on the last nucleotide of exon 6(*23*) (termed G790A in this study) (Fig. 4A). Firstly, we confirmed the hypertrophy phenotype of G790A mice and determine the zerumbone administration time. As shown in Supplementary Fig. 10, homozygous (Ki/Ki) mice exhibited certain signs of cardiac hypertrophy at week 5 after birth, such as increased IVSd, LVPWd and LVMI indexes, while heterozygotes (Ki/WT) did not show significant symptoms of cardiac hypertrophy in early stage and was consistent to previous report (*23, 24*). However, considering the lactation of mice, we chose mice

at 4-6 weeks as our experimental subjects for therapeutic treatment of zerumbone. Male mice at 4-6 weeks were treated with processed feedstuff containing 0.07% zerumbone for 32 weeks. KI (homozygote) mice exhibited LV hypertrophy compared to WT with a significant increase of heart size, heart weight/body weight ratio, cardiomyocytes cross-sectional area, as well as improvement in echocardiographic data, including IVSd, LVPWd and LVMI (Fig. 4B-4F, Supplementary Fig. 11B, Supplementary Table 6). Upregulation of fetal genes (*β-MHC*, *BNP* and *ANP*) and cardiac function related gene (*MEF2C*) were also observed in G790A-KI male mice (Fig. 4F, Supplementary Fig. 11). The aggravation of fibrosis and induction of collagen I were also observed in G790A-KI male mice. Furthermore, treatment of zerumbone also prevented the induction of collagen I and showed a falling trend in fibrosis, but the difference was not significant (Fig. 4E, 4G). And, no significant differences were observed in the heart between WT-blank and WT-Zer treated groups. In contrast, these hypertrophic growth features were substantially suppressed by zerumbone treatment (Fig. 4, Supplementary Fig. 11). In addition, studies of zerumbone in female HCM mice resulted in a similar conclusion observed in male HCM mice (Supplementary Fig. 12 and Supplementary Table 7). Collectively, our data demonstrated that zerumbone was able to repress cardiac hypertrophy in HCM mice.

Zerumbone activates NRF2 signaling with a highly efficient induction of HO-1

To explore the detailed molecular mechanisms of repressing cardiac hypertrophy by zerumbone, we first used whole transcriptomic RNA sequencing to pick up differentially expressed genes in hESC-CMs treated with zerumbone in a short time of 3h. We identified 19 genes that were significantly upregulated, and almost half of these upregulated genes (9/19) belonged to the downstream of NRF2 target genes (Fig. 5A-5B). In particular, both gene set enrichment analysis (GSEA) and heap map indicated that NRF2 pathway was activated in zerumbone treated cardiomyocytes (Fig. 5C-5D). Among the up-regulated genes, *HMOX1* was the most significantly upregulated (Fig. 5B, 5D) one. The expression changes of NRF2 target transcripts were further validated by RT-PCR with additional time points (Fig. 5E, Supplementary Fig. 13A). Zerumbone induced up-regulation of transcript levels of *HMXO1* and *NQO1*, as well as other NRF2 downstream targets, including *MAFG, HSPA1A, DNAJB1, TXNRD1and SRXN1*. Zerumbone treatment caused an accumulation of NRF2 protein both in the total cell lysates and the nuclear extract from hESC-CMs (Fig. 5F-5G). The expression of NQO1 was also increased at 24h after zerumbone treatment (Fig. 5F). However, the mRNA expression of KEAP1 and NRF2 were inconsistent with its protein expression. This may due to more complex post-transcriptional regulation or protein modification. Most notably, the mRNA level of *HMOX1* was increased by nearly 100 times than that of the control (Fig. 5E). Consistently, zerumbone led to a dose-dependent and time-dependent upregulation of HO-1 protein in hESC-CMs (Fig. 5H-5I). Surprisingly, we observed that HO-1 induction of zerumbone was much higher than the classical HO-1 inducer hemin (Fig. 5J-5K). As HO-1 plays a crucial protective effect on cardiac maladaptation and hypertrophy(*10, 11, 25*), we next further investigated whether zerumbone could induce HO-1 in *vivo*. Oral dosing of C57 with zerumbone (70 mg/kg) also induced HO-1 and NRF2 expression in heart tissues at 24h after intragastric administration (Fig. 5L-5N). Similar activation of NRF2/HO-1 signaling was also observed in another cardiac myocyte cell line AC16 (Supplementary Fig. 13C-13F).

HO-1 induction is regulated by multiple transcription factors, including NRF2 and HSF1(*26*). Heat shock response is accompanied with activation of HSF1 by trimerization after phosphorylation(*27*). Hence, we set up to examine whether zerumbone can induce HSF1 activation. As shown in Supplementary Fig. 14, zerumbone caused a significant accumulation of HSF1 in the nuclei and increased phosphorylation of HSF1 both in the total lysates and nuclei from hESC-CMs or AC16 cells. Zerumbone also led to a dose-dependent upregulation of p-HSF1 in the total lysates and accumulation of HSF1 in the nuclei (Supplementary Fig. 14B-14C, 14F). The intracellular GSSG levels was reduced with zerumbone treatment for 6h, while the GSH levels did not show significant difference (Supplementary Fig. 14G). With the activation of HO-1 and NRF2, oxidation was not caused by zerumbone treatment for 6h.

Next, we further investigated whether upregulation of HO-1 induced by zerumbone is also affected by HSF1. To confirm our conclusion, we silenced NRF2 or/and HSF1 with siRNA in hESC-CMs. With an obviously reduced expression of NRF2 or/and HSF1 mRNA and protein levels, induction of HO-1 was heavily weakened only by the downregulation of NRF2 (Fig. 5O-5U). These results indicated that, although zerumbone could activate HSF1, but the marked upregulation of HO-1 by zerumbone was mainly via the activation of NRF2 rather than HSF1. Thus, these results suggested that zerumbone could activate NRF2 signaling pathway both *in vitro* and *in vivo* with a highly efficient induction of HO-1 expression.

Zerumbone triggers a formation of HMW KEAP1 and activates NRF2 pathway through CUL3-dependent inhibition of NRF2 ubiquitination

KEAP1, a member of BTB-Kelch protein family, is a key repressor of NRF2 activity and substrate adaptor protein to a CUL3-dependent E3 ubiquitin ligase complex(*28-30*). As the N-terminal BTB domain of KEAP1 binds to CUL3 and the C-terminal Kelch domain of KEAP1 binds to NRF2, expression of NRF2 is primarily controlled by the KEAP1/CUL3 E3 ubiquitin ligase complex through ubiquitination and proteasomal degradation of NRF2(*31, 32*). Previous studies reported that a wide range of electrophiles and oxidants could modify cysteine in KEAP1 and disrupt the formation of CUL3-dependent E3 ubiquitin ligase complex, leading to accumulation and translocation of NRF2 with the inhibition of ubiquitination(*33-35*).

In order to explore the mechanism of zerumbone inducing the activation of NRF2, we first investigated whether zerumbone could directly bind to KEAP1. As shown in Fig. 6A, SPR analysis indicated that zerumbone directly bound to KEAP1 with a KD of 25.6 μM. Treatment of hESC-CMs with 30 μM zerumbone for 4h at 37°C resulted in an inhibition of endogenous interaction of CUL3 and KEAP1 (Figure 6B). Meanwhile, zerumbone also disrupted the interaction between exogenous overexpressed CUL3 and KEAP1 protein in 293T transfected with FLAG-KEAP1 and MYC-CUL3 plasmids (Fig. 6C). With zerumbone treatment, we observed an increase in a series of high molecular weight (HMW) KEAP1 bands with a molecular weight greater than 150 kDa and a reduction in KEAP1 monomer band with molecular weight of 70 kDa (Fig. 6B-6D). Hong et al. found that the HMW KEAP1 was modified by K-48-linked polyubiquitin conjugates, which coincided with NRF2 stabilization and translocation(*36*). As cysteines are rich in KEAP1 and play a crucial role in NRF2 activation by canonical inducer like tBHQ(*35, 37*), we mutated

those cysteines related to the interaction with CUL3 to alanine or serine in the BTB domain of KEAP1. However, those cysteine mutants failed to inhibit zerumbone-induced formation of HMW KEAP1 as well as upregulation of HO-1 and NRF2 proteins (Fig. 6D, Supplementary Fig. 15A). When Cys 151 was mutated, the HMW KEAP1 bands were disappeared, which suggested that Cys 151 played a key role in the formation of HMW KEAP1 as previous studies reported(*38, 39*) (Figure 6D). Our data indicated that the disruption in the interaction between KEAP1 and CUL3 of zerumbone was not dependent on the several key cysteines in the BTB domain of KEAP1. Most canonical electrophiles can covalently bound to KEAP1 through interacting with the thiol groups in cysteine and then induce the activation of NRF2 signaling(*40*). Generally, this effect can be suppressed by the addition of some reductants containing thiol groups, like DTT or GSH(*41, 42*). As shown in Supplementary Fig. 15B-15C, DTT or GSH (1 mM) pretreatment showed no effect on the zerumbone-induced upregulation of NRF2 both in total lysates and the nuclei extract, while HO-1 was significantly downregulated. Meanwhile, an excessive dose of DTT or GSH (500 μM) pretreatment showed slightly lower amount of HMW KEAP1 induced by (15 μM) zerumbone (Supplementary Fig. 15E). High dose of DTT or GSH pretreatment still can't fully prevent the formation of HMW KEAP1 and activation of NRF2 induced by zerumbone. It suggested that the modification of cysteine(s) played a role in the formation of HMW KEAP1 which was consistent with our previous finding that the HMW KEAP1 was fully inhibited with Cys 151 mutation (Fig. 6D). Zerumbone exhibited a strong effect on NRF2 activation even in the massive presence of reductants like DTT or GSH, while the downregulation of HO-1 may be caused by the stronger antioxidative effect of reductant on the downstream of NRF2.

On the other hand, the dissociation of NRF2 and KEAP1 can also induce the NRF2 accumulation and translocation. To address this possibility, we first examined the NRF2 in nuclei and cytoplasm in hESC-CMs after treated with different combination of zerumbone, CHX (protein synthesis inhibitor), and MG132 (proteasome inhibitor). While the upregulation of NRF2 in nuclei was induced 1h after zerumbone treatment, the induction of NRF2 was largely abolished in the presence of CHX (Fig. 6E). And when treated with MG132 to inhibit the degradation of NRF2, it caused a similar effect on the induction of NRF2 like zerumbone. Similar results were obtained in 3h and 6h treatment of CHX or MG132 (Supplementary Fig. 15D). These results suggested that accumulation of NRF2 in the nuclei was related to the newly synthesized NRF2 rather than the NRF2 liberated from KEAP1, and also related to the inhibition of NRF2 ubiquitination. We further analyzed the effect of zerumbone on the interaction of NRF2 and KEAP1. When we treated hESC-CMs or 293T cells (NRF2 and KEAP1 overexpressed) with zerumbone for 4h before harvest, the protein level of NRF2 in lysates was much higher than that of the control (Supplementary Fig. 15H-15I), and this hindered us from observing the actual interaction between NRF2 and KEAP1. Thus, we incubated zerumbone in *vitro* at 4°C for 3h after harvesting cell lysates from 293T (NRF2 and KEAP1 overexpressed), and further confirmed that zerumbone disrupted the interaction between CUL3 and KEAP1 (Supplementary Fig. 15F-15G) rather than affecting the interaction between NRF2 and KEAP1 (Fig. 6F, Supplementary Fig. 15J). We also assessed the half-time and ubiquitination of NRF2. We observed a significant increased half-time (from 24.4 min to 55.1 min) and decreased ubiquitination of NRF2 after zerumbone treatment (Fig. 6G-6H). Conclusively, these results demonstrated

that zerumbone could trigger a formation of HMW KEAP1 and activate the NRF2 pathway through CUL3-dependent inhibition of ubiquitination.

Downregulation of HO-1 blunts the cardioprotective effect of zerumbone in cardiac hypertrophy

NRF2/HO-1 signaling has been demonstrated as a crucial mediator in cytoprotective defense against cardiac maladaptation and hypertrophy(*10, 11*). Induction of HO-1 showed a cardioprotective effect on hypertrophic cardiomyocytes induced by angiotension II or hyperglycemia and improved pathological remodeling of left ventricular in heart failure(*43-45*). And, activation of NRF2 attenuated diabetic cardiomyopathy by upregulation of HO-1 in mice with type I diabetes(*46*). To further confirm the contribution of zerumbone in alleviating cardiac hypertrophy is via the NRF2/HO-1 signaling, we used a HO-1 inhibitor, HO-1-IN-1 to observe the anti-hypertrophic effect of zerumbone in *vitro*(*47*). The upregulation of HO-1 in zerumbone treated cardiomyocytes was inhibited with 1 μM or 5 μM HO-1-IN-1 (Fig. 7A). While zerumbone reduced NE-induced enlargement of cell area, HO-1-IN-1 abolished this effect of zerumbone with a significant increase of cell size (Fig. 7B). In cardiomyocytes functional assays, we observed a shorter frequency and reduced duration of calcium transients, including time to peak and decay time, as well as increased transient amplitudes with HO-1-IN-1 treatment compared to zerumbone treated group (Fig. 7D-7I). Meanwhile, the contraction force was enhanced with the addition of HO-1-IN-1 (Fig. 7J-7K). These data indicated that downregulation of HO-1 partially abolished the anti-hypertrophic effect of zerumbone in cardiomyocytes treated with NE.

Conclusively, we identified zerumbone as a new effective agent for cardiac hypertrophy through high-throughput screening. Zerumbone can directly bind to KEAP1 and impede the interaction between CUL3 and KEAP1, leading to the accumulation of NRF2 through inhibiting the ubiquitination of NRF2. The translocation of NRF2 into nuclei induces a marked upregulation of HO-1 and results in a significant cardioprotective effect in cardiac hypertrophy (Fig. 8).

Discussion

Cardiac hypertrophy has become a global health problem and life-threatening occurrence with a higher incidence, which increases the risk of stroke, heart failure, and premature death(*48, 49*). However, existing pharmacologic therapies only provide some symptom relief. No specific drugs that alter the disease progression or prevent cardiac dysfunction in late stage has been developed(*50, 51*). For patients with hypertension, antihypertensive drugs could be a preferred option, but for HCM patients, none existing drugs show satisfied clinical effects. There is only one candidate drug, MYK-461, now in phase III clinical trials, showing a potential better therapeutic effect for hypertrophic obstructive cardiomyopathy(*50*). Here, by high-throughput drug screening, we identified that zerumbone, a natural active ingredient isolated from the tropical plant *Zingiber zerumbet*, showed a therapeutic effect for cardiac hypertrophy both in HCM and hypertension.

As cardiomyocytes are terminally differentiated cells, it is hard to proliferate in *vitro* under normal physiological conditions. However, cell-based drug screening assays have heavily relied on immortalized

cell lines. As a result, the discovery of novel cardiovascular drugs has historically been hindered by the limited availability of cardiomyocytes and cell models that could accurately reflect the pathological profile of cardiovascular disease(*52, 53*). The development of iPSCs and differentiation technology provided an indefatigable source of cardiomyocytes and convenient platform for cardiovascular drug screening. Although various cell models of heart diseases have been generated using iPSCs or hESCs, such as dilated cardiomyopathy (DCM)(*54*), hypertrophic cardiomyopathy (HCM)(*55*), arrhythmogenic right ventricular dysplasia (ARVD)(*56, 57*) and so on, very few of them have been successfully translated into the platform for high-throughput drug screening(*58, 59*). This may be due to the unstable cardiac differentiation efficiency limits the establishment of large-scale drug screening based on cellular phenotypes. Non-myocytes quickly proliferate and may raise interfering signals and disturb the stability of the whole screening system. Relevant to a previous study from Kondo and his colleagues, they differentiated neurons from iPSCs derived from patients with Alzheimer's disease with nearly 100% purity after selected with Dox, and then established a robust screening system based on the assay for amyloid β peptide(*60*). In this study, we introduced a purification step to cardiomyocytes derived from $MYL2^{Neo/WT}$-H7 cell line. High purity of cardiomyocytes laid a solid foundation for the subsequent high-content imaging analysis and contributed to establishing a stable large-scale screening system. Of note, we established for the first time a high-throughput screen system based on the NE-induced cardiac hypertrophy model of purified hESC-CMs.

Zerumbone, a sesquiterpene isolated from *Zingiber zerumbet Smith*, has been reported to exhibit a wide range of biological activities, including anti-inflammation(*61*), anti-oxidation(*62*), anti-tissues injury(*63*), anti-cancer activities(*64*). Previous studies showed that zerumbone could induce HO-1 expression both in epidermal cells and in skin(*65*) and exhibited extensive protective effect on multiple organ damages(*63, 66, 67*). However, the molecular and biochemical mechanism of how zerumbone activate NRF2/HO-1 signaling and whether it has cardioprotective activity has not been well elucidated. Here, we found that zerumbone showed a marked induction of HO-1 in cardiomyocytes and exhibited an anti-hypertrophic effect both in *vitro* and *in vivo*. We further proved that zerumbone directly bound to KEAP1 and impeded the interaction between CUL3 and KEAP1, leading to the accumulation of NRF2 through inhibiting its ubiquitination (Fig. 6). Zerumbone was previously reported to covalently bound to KEAP1(*68*). In this study, we presented more detailed data and showed that zerumbone directly bound to KEAP1. However, the specific binding mode and binding site of zerumbone to KEAP1 still needs to be further investigated.

It is widely accepted that activation of NRF2/HO-1 signaling represents an adaptive response resistant to oxidative injury and plays a crucial role in various pathological conditions including cardiac hypertrophy(*69-71*). Many studies have shown that induction of HO-1 could inhibit cardiac hypertrophy both in *vitro* and *vivo*(*44, 70, 72-76*). We also validated that the anti-hypertrophic effect of zerumbone in cardiomyocytes was suppressed by the downregulation of HO-1 (Fig. 7). And whether this anti-hypertrophic effect could be abolished in *vivo* by inhibiting HO-1 still needs further study, as well as the toxicity raised by zerumbone treatment in other organs warrant further investigation.

In conclusion, we have established a high-throughput drug screening system based on hESC-derived CMs in searching for effective treatment for cardiac hypertrophy. This powerful screening platform has shown great potential to discover more new drugs for cardiac hypertrophy treatment. We identified zerumbone as an effective agent for cardiac hypertrophy both in *vitro* and *vivo* through marked upregulation of HO-1 expression. Our study provide evidence that zerumbone directly interacts with KEAP1 and disturbs its interaction with CUL3. Zerumbone induces the activation of NRF2/HO-1 signaling through inhibiting the ubiquitination of NRF2. These data support the concept that NRF2/HO-1 could serve as a possible drug therapy target for cardiac hypertrophy. Our data also showed that inhibition of hypertrophy by zerumbone was not dependent on blood pressure lowering. Zerumbone could be used in combination with current antihypertensive drugs for hypertension patients with cardiac hypertrophy and could also be used in treatments for patients of inherited hypertrophic cardiomyopathy in the future.

Methods

Culture and cardiac differentiation

The human H7 hESCs (Wicell Research Institute) were cultured with mTeSR medium (STEMCELL Technologies, Cat#85851 and 85852) on Matrigel-coated (Corning, Cat#356231) plates. hESCs were digested with Accutase (Sigma, Cat#A6964) and maintained at 37 °C with 5% CO_2. Cardiac differentiation was performed according to a previously described protocol with minor modifications(*77, 78*). The CMs (day 25-30 after differentiation) were dissociated with Collagenase I (Sigma, Cat#SCR103) and 0.05% EDTA/Trypsin (Sigma, Cat#59417C), and cultured with 5-10% FBS/DMEM for subsequent screening, functional, and molecular assays.

High throughput drug screening

Day 25 post-differentiation hESC-CMs were purified with G418 (100 μg/ml) for 5 days and digested with Collagenase I for 1h and 0.05% EDTA/Trypsin for 5-10 min. Dissociated CMs were suspended with 5% FBS/DMEM and filtered with a 40 μm cell strainer (BD Falcon, Cat#352340) to remove large cell clumps. CMs were plated at 1,400 cells per well in 384-well plates (PerkinElmer, Cat#6007460) in 45 μl 5% FBS/DMEM medium with a Multidrop Combi (Thermo Fisher Scientfic). Cells were then centrifuged at 600 rpm for 1 min and cultured at 37 °C with 5% CO_2.

The natural compounds library was obtained from Chemical Biology Core Facility of the Shanghai Institute of Biochemistry and Cell Biology, Chinese Academy of Sciences. All compounds were dissolved in DMSO as 10 mM stocks in 96-well plate (U-shaped bottom, Corning, Cat#3879) and then diluted with DMEM to 100 μM with a Multidrop Combi. For each 96-well compound plate, vehicle controls (1% DMSO/DMEM); negative controls (200 μM NE/DMEM), and positive controls (200 μM prazosin/DMEM) were included. No treatment was performed to the outer circle of the 96-well plates. After 24h seeding of CMs, compounds from the library plates were reformatted into 384-well cell plates using a Bravo Automated Liqid Handling Platform (Agilent). Each compound was screened for 4 duplicate wells at 5

μl/well with a final concentration of 10 μM. Following 3h of drug pretreatment, NE was added into each well with a Multidrop Combi at a volume of 5.6 μl/well. For negative (with only NE treatment) or positive controls (with prazosin treatment), the final assay concentration was both 20 μM. And there was no drug treatment on the periphery of all the 384-well plates.

After 5 days treatment, CMs grown on 384-well plates were washed 3 times with preheated (37 °C) PBS solution using a Microplate Washer Elx405 (Bio Tek) and then labeled with CellTracker Deep Red Dye (Invitrogen, Cat#C34565) at 37 °C for 1h. CellTracker was added with the Multidrop Combi at a final concentration of 5 μM. Following washing with PBS, CMs were fixed with 4% paraformaldehyde for 30 min, permeabilized for 20 min with PBST (containing 0.1% Triton-X100, and incubated with the primary antibody cTNT (1:500, Thermo Fisher Scientific, Cat#MA5-12960) at 4 °C overnight. After washed with PBST for 6 times, CMs were incubated simultaneously for 1h with the AlexaFluor488 conjugated secondary antibody (1:300, Thermo Fisher Scientific, Cat#A-11001) and DAPI (1:1000, Sigma, Cat#D9542) in 1% BSA/PBST. Cells were then washed 6 times with PBST and imaged. The secondary screen was performed with the same assay conditions as the primary screen.

High content imaging and analysis

All images were collected using the Operetta imaging system (PerkinElmer) under the 10x objective with 3 fields/well captured. Image analysis was performed with the Harmony software. Briefly, first, the nuclei was identified with DAPI signaling using standard nuclei detection modules (filter for nucleus intensity>500 and roundness>0.5). Second, the cytoplasm was identified with CellTracker staining signaling with removement of border objects. Third, CMs were identified with cTnT staining signaling, and cell area was calculated with membrane region removed (-10% of outer border~10% of inner border). The mean area of CMs between 1000 μm^2 and 4000 μm^2 were defined as small CMs, while the mean area of CMs between 4000 μm^2 and 20000 μm^2 were defined as large CMs. The ratio of small and large CMs represent the percentage of the total number of CMs. Output for CMs with area <1000 μm^2 was due to the undigested clumps or background. Output for CMs with area >20000 μm^2 was from inaccurate recognition of multinuclear CMs as one cardiomyocyte. These parts of data were not counted in. In order to be counted as positive hits, compounds must show a significant difference to NE treated wells with *P* value less than 0.05 both on 3 screening indexes (mean area, small CMs ratio, and large CMs ratio). In addition, the compounds that showed a reduced cell number based on DAPI counting by more than 40% were ruled out, which was likely due to cellular toxicity.

Statistical analysis

All data were presented as mean ± SEM. Comparison between two groups were evaluated using unpaired two-tailed Student's *t*-test. Comparison among multiple groups were evaluated by one-way analysis of variance (ANOVA). Data were considered statistically significant when *P* value <0.05. All data calculations were analyzed using Prism 7 software (GraphPad). All in *vivo* and *vitro* experiments were repeated multiple times with multiple batches of rats, mice, and cell samples as indicated in figure legends.

Declarations

Acknowledgements

This work was supported by the National Natural Science Foundation of China (NSFC No.82070391, N.S.), the Young Elite Scientist Sponsorship Program by CAST (2018QNRC001), the Haiju program of National Children's Medical Center EK1125180102, and the National Key R&D Program of China 2018YFC2000202 (N.S.). We apologize to people whose work was relevant to but not cited in this study due to limited space.

Author contributions:

JH and NS contributed to manuscript writing and experimental design. JH, LQ, ZXX, XYL and JXC performed the experiment and analyzed data. HYC contributed to echocardiography and data analysis. QYZ and WJZ gave assistance to animal experiment. SJL, SH, HWZ and YQC gave technical assistance in drug screening and SPR assay. EML and XYC contributed to data analysis. SJL, CX, CL and XBL provided advices on experimental design. SFC and RZQ contributed to manuscript review and editing.

Conflict of interests: The authors declare that they have no competing interests.

References

1. C. Cuspidi *et al.*, High Normal Blood Pressure and Left Ventricular Hypertrophy Echocardiographic Findings From the PAMELA Population. *Hypertension* **73**, 612-619 (2019).

2. B. J. Maron *et al.*, Prevalence of hypertrophic cardiomyopathy in a general population of young adults. Echocardiographic analysis of 4111 subjects in the CARDIA Study. Coronary Artery Risk Development in (Young) Adults. *Circulation* **92**, 785-789 (1995).

3. G. G. Schiattarella, J. A. Hill, Inhibition of hypertrophy is a good therapeutic strategy in ventricular pressure overload. *Circulation* **131**, 1435-1447 (2015).

4. H. Ma *et al.*, Lin28a Regulates Pathological Cardiac Hypertrophic Growth Through Pck2-Mediated Enhancement of Anabolic Synthesis. *Circulation* **139**, 1725-1740 (2019).

5. P. K. Whelton *et al.*, 2017 ACC/AHA/AAPA/ABC/ACPM/AGS/APhA/ASH/ASPC/NMA/PCNA Guideline for the Prevention, Detection, Evaluation, and Management of High Blood Pressure in Adults: A Report of the American College of Cardiology/American Heart Association Task Force on Clinical Practice Guidelines. *Hypertension* **71**, e13-e115 (2018).

6. M. R. Mehra, P. A. Uber, G. S. Francis, Heart failure therapy at a crossroad: are there limits to the neurohormonal model? *J Am Coll Cardiol* **41**, 1606-1610 (2003).

7. J. C. Del Álamo *et al.*, High throughput physiological screening of iPSC-derived cardiomyocytes for drug development. *Biochim Biophys Acta* **1863**, 1717-1727 (2016).

8. N. M. Mordwinkin, P. W. Burridge, J. C. Wu, A review of human pluripotent stem cell-derived cardiomyocytes for high-throughput drug discovery, cardiotoxicity screening, and publication standards. *J Cardiovasc Transl Res* **6**, 22-30 (2013).

9. A. Sharma *et al.*, Use of human induced pluripotent stem cell-derived cardiomyocytes to assess drug cardiotoxicity. *Nat Protoc* **13**, 3018-3041 (2018).

10. J. Li *et al.*, Nrf2 protects against maladaptive cardiac responses to hemodynamic stress. *Arterioscler Thromb Vasc Biol* **29**, 1843-1850 (2009).

11. P. Nie, F. Meng, J. Zhang, X. Wei, C. Shen, Astragaloside IV Exerts a Myocardial Protective Effect against Cardiac Hypertrophy in Rats, Partially via Activating the Nrf2/HO-1 Signaling Pathway. *Oxid Med Cell Longev* **2019**, 4625912 (2019).

12. B. Li *et al.*, Engineering human ventricular heart muscles based on a highly efficient system for purification of human pluripotent stem cell-derived ventricular cardiomyocytes. *Stem Cell Res Ther* **8**, 202 (2017).

13. U. Subramanian *et al.*, Retinoic acid and sodium butyrate suppress the cardiac expression of hypertrophic markers and proinflammatory mediators in Npr1 gene-disrupted haplotype mice. *Physiol Genomics* **48**, 477-490 (2016).

14. X. Dong *et al.*, Downregulation of miR-21 is involved in direct actions of ursolic acid on the heart: implications for cardiac fibrosis and hypertrophy. *Cardiovasc Ther* **33**, 161-167 (2015).

15. X. T. Wang *et al.*, Ursolic acid ameliorates oxidative stress, inflammation and fibrosis in diabetic cardiomyopathy rats. *Biomed Pharmacother* **97**, 1461-1467 (2018).

16. Z. L. Yang *et al.*, [Effect of ursolic acid on cardiomyopathy of mice with diabetes and its mechanism]. *Zhongguo Ying Yong Sheng Li Xue Za Zhi* **34**, 309-312 339 (2018).

17. J. C. Doxey, A. C. Lane, A. G. Roach, N. K. Virdee, Comparison of the alpha-adrenoceptor antagonist profiles of idazoxan (RX 781094), yohimbine, rauwolscine and corynanthine. *Naunyn Schmiedebergs Arch Pharmacol* **325**, 136-144 (1984).

18. G. Goel, H. P. Makkar, G. Francis, K. Becker, Phorbol esters: structure, biological activity, and toxicity in animals. *Int J Toxicol* **26**, 279-288 (2007).

19. X. L. Zhang, L. Wang, F. Li, K. Yu, M. K. Wang, Cytotoxic phorbol esters of Croton tiglium. *J Nat Prod* **76**, 858-864 (2013).

20. M. Dewenter, A. von der Lieth, H. A. Katus, J. Backs, Calcium Signaling and Transcriptional Regulation in Cardiomyocytes. *Circ Res* **121**, 1000-1020 (2017).

21. D. M. Bers, Calcium cycling and signaling in cardiac myocytes. *Annu Rev Physiol* **70**, 23-49 (2008).

22. B. J. Wilkins, J. D. Molkentin, Calcium-calcineurin signaling in the regulation of cardiac hypertrophy. *Biochem Biophys Res Commun* **322**, 1178-1191 (2004).

23. N. Vignier *et al.*, Nonsense-mediated mRNA decay and ubiquitin-proteasome system regulate cardiac myosin-binding protein C mutant levels in cardiomyopathic mice. *Circ Res* **105**, 239-248 (2009).

24. C. N. Toepfer *et al.*, Hypertrophic cardiomyopathy mutations in MYBPC3 dysregulate myosin. *Sci Transl Med* **11**, (2019).

25. P. Velusamy *et al.*, Targeting the Nrf2/ARE Signalling Pathway to Mitigate Isoproterenol-Induced Cardiac Hypertrophy: Plausible Role of Hesperetin in Redox Homeostasis. *Oxid Med Cell Longev* **2020**, 9568278 (2020).

26. S. Inouye *et al.*, NRF2 and HSF1 coordinately regulate heme oxygenase-1 expression. *Biochem Biophys Res Commun* **506**, 7-11 (2018).

27. R. Akagi, T. Kubo, Y. Hatori, T. Miyamoto, S. Inouye, Heme oxygenase-1 induction by heat shock in rat hepatoma cell line is regulated by the coordinated function of HSF1, NRF2 and BACH1. *J Biochem* **170**, 501-510 (2021).

28. S. C. Lo, M. Hannink, PGAM5, a Bcl-XL-interacting protein, is a novel substrate for the redox-regulated Keap1-dependent ubiquitin ligase complex. *J Biol Chem* **281**, 37893-37903 (2006).

29. K. L. Thu *et al.*, Genetic disruption of KEAP1/CUL3 E3 ubiquitin ligase complex components is a key mechanism of NF-kappaB pathway activation in lung cancer. *J Thorac Oncol* **6**, 1521-1529 (2011).

30. D. D. Zhang *et al.*, Ubiquitination of Keap1, a BTB-Kelch substrate adaptor protein for Cul3, targets Keap1 for degradation by a proteasome-independent pathway. *J Biol Chem* **280**, 30091-30099 (2005).

31. S. B. Cullinan, J. D. Gordan, J. Jin, J. W. Harper, J. A. Diehl, The Keap1-BTB protein is an adaptor that bridges Nrf2 to a Cul3-based E3 ligase: oxidative stress sensing by a Cul3-Keap1 ligase. *Mol Cell Biol* **24**, 8477-8486 (2004).

32. K. Itoh *et al.*, Keap1 regulates both cytoplasmic-nuclear shuttling and degradation of Nrf2 in response to electrophiles. *Genes Cells* **8**, 379-391 (2003).

33. C. A. Silva-Islas, P. D. Maldonado, Canonical and non-canonical mechanisms of Nrf2 activation. *Pharmacol Res* **134**, 92-99 (2018).

34. K. Taguchi, H. Motohashi, M. Yamamoto, Molecular mechanisms of the Keap1–Nrf2 pathway in stress response and cancer evolution. *Genes Cells* **16**, 123-140 (2011).

35. A. T. Dinkova-Kostova, R. V. Kostov, P. Canning, Keap1, the cysteine-based mammalian intracellular sensor for electrophiles and oxidants. *Arch Biochem Biophys* **617**, 84-93 (2017).

36. F. Hong, K. R. Sekhar, M. L. Freeman, D. C. Liebler, Specific patterns of electrophile adduction trigger Keap1 ubiquitination and Nrf2 activation. *J Biol Chem* **280**, 31768-31775 (2005).

37. X. He, Q. Ma, Critical cysteine residues of Kelch-like ECH-associated protein 1 in arsenic sensing and suppression of nuclear factor erythroid 2-related factor 2. *J Pharmacol Exp Ther* **332**, 66-75 (2010).

38. T. Ohnuma *et al.*, Activation of the Nrf2/ARE pathway via S-alkylation of cysteine 151 in the chemopreventive agent-sensor Keap1 protein by falcarindiol, a conjugated diacetylene compound. *Toxicol Appl Pharmacol* **244**, 27-36 (2010).

39. K. R. Sekhar, G. Rachakonda, M. L. Freeman, Cysteine-based regulation of the CUL3 adaptor protein Keap1. *Toxicol Appl Pharmacol* **244**, 21-26 (2010).

40. X. Wei, H. Yin, Covalent modification of DNA by α, β-unsaturated aldehydes derived from lipid peroxidation: Recent progress and challenges. *Free Radic Res* **49**, 905-917 (2015).

41. I. Almazari *et al.*, Guggulsterone induces heme oxygenase-1 expression through activation of Nrf2 in human mammary epithelial cells: PTEN as a putative target. *Carcinogenesis* **33**, 368-376 (2012).

42. H. H. Lee *et al.*, Piceatannol induces heme oxygenase-1 expression in human mammary epithelial cells through activation of ARE-driven Nrf2 signaling. *Arch Biochem Biophys* **501**, 142-150 (2010).

43. J. Xu *et al.*, Propofol ameliorates hyperglycemia-induced cardiac hypertrophy and dysfunction via heme oxygenase-1/signal transducer and activator of transcription 3 signaling pathway in rats. *Crit Care Med* **42**, e583-594 (2014).

44. C. M. Hu, Y. H. Chen, M. T. Chiang, L. Y. Chau, Heme oxygenase-1 inhibits angiotensin II-induced cardiac hypertrophy in vitro and in vivo. *Circulation* **110**, 309-316 (2004).

45. G. Wang *et al.*, Cardioprotective and antiapoptotic effects of heme oxygenase-1 in the failing heart. *Circulation* **121**, 1912-1925 (2010).

46. Y. Wang *et al.*, Therapeutic effect of MG-132 on diabetic cardiomyopathy is associated with its suppression of proteasomal activities: roles of Nrf2 and NF-κB. *Am J Physiol Heart Circ Physiol* **304**, H567-578 (2013).

47. G. Floresta *et al.*, Development of new HO-1 inhibitors by a thorough scaffold-hopping analysis. *Bioorg Chem* **81**, 334-339 (2018).

48. D. Levy, R. J. Garrison, D. D. Savage, W. B. Kannel, W. P. Castelli, Prognostic implications of echocardiographically determined left ventricular mass in the Framingham Heart Study. *N Engl J Med* **322**, 1561-1566 (1990).

49. B. J. Maron *et al.*, Clinical course of hypertrophic cardiomyopathy in a regional United States cohort. *Jama* **281**, 650-655 (1999).

50. E. M. Green *et al.*, A small-molecule inhibitor of sarcomere contractility suppresses hypertrophic cardiomyopathy in mice. *Science* **351**, 617-621 (2016).

51. R. Spoladore, M. S. Maron, R. D'Amato, P. G. Camici, I. Olivotto, Pharmacological treatment options for hypertrophic cardiomyopathy: high time for evidence. *Eur Heart J* **33**, 1724-1733 (2012).

52. P. Horvath *et al.*, Screening out irrelevant cell-based models of disease. *Nat Rev Drug Discov* **15**, 751-769 (2016).

53. M. A. Cayo *et al.*, A Drug Screen using Human iPSC-Derived Hepatocyte-like Cells Reveals Cardiac Glycosides as a Potential Treatment for Hypercholesterolemia. *Cell Stem Cell* **20**, 478-489.e475 (2017).

54. C. McDermott-Roe *et al.*, Investigation of a dilated cardiomyopathy-associated variant in BAG3 using genome-edited iPSC-derived cardiomyocytes. *JCI Insight* **4**, (2019).

55. L. Han *et al.*, Study familial hypertrophic cardiomyopathy using patient-specific induced pluripotent stem cells. *Cardiovasc Res* **104**, 258-269 (2014).

56. A. Khudiakov *et al.*, Generation of iPSC line from patient with arrhythmogenic right ventricular cardiomyopathy carrying mutations in PKP2 gene. *Stem Cell Res* **24**, 85-88 (2017).

57. J. Y. Wen *et al.*, Maturation-Based Model of Arrhythmogenic Right Ventricular Dysplasia Using Patient-Specific Induced Pluripotent Stem Cells. *Circ J* **79**, 1402-1408 (2015).

58. A. Sharma *et al.*, High-throughput screening of tyrosine kinase inhibitor cardiotoxicity with human induced pluripotent stem cells. *Sci Transl Med* **9**, (2017).

59. M. Csöbönyeiová, Š. Polák, L. Danišovič, Toxicity testing and drug screening using iPSC-derived hepatocytes, cardiomyocytes, and neural cells. *Can J Physiol Pharmacol* **94**, 687-694 (2016).

60. T. Kondo *et al.*, iPSC-Based Compound Screening and In Vitro Trials Identify a Synergistic Anti-amyloid β Combination for Alzheimer's Disease. *Cell Rep* **21**, 2304-2312 (2017).

61. M. A. Haque, I. Jantan, L. Arshad, S. N. A. Bukhari, Exploring the immunomodulatory and anticancer properties of zerumbone. *Food Funct* **8**, 3410-3431 (2017).

62. A. Murakami *et al.*, Zerumbone, a Southeast Asian ginger sesquiterpene, markedly suppresses free radical generation, proinflammatory protein production, and cancer cell proliferation accompanied by apoptosis: the alpha,beta-unsaturated carbonyl group is a prerequisite. *Carcinogenesis* **23**, 795-802 (2002).

63. W. S. Leung *et al.*, Protective effect of zerumbone reduces lipopolysaccharide-induced acute lung injury via antioxidative enzymes and Nrf2/HO-1 pathway. *Int Immunopharmacol* **46**, 194-200 (2017).

64. H. S. Rahman *et al.*, Biomedical properties of a natural dietary plant metabolite, zerumbone, in cancer therapy and chemoprevention trials. *Biomed Res Int* **2014**, 920742 (2014).

65. J. W. Shin *et al.*, Zerumbone induces heme oxygenase-1 expression in mouse skin and cultured murine epidermal cells through activation of Nrf2. *Cancer Prev Res (Phila)* **4**, 860-870 (2011).

66. N. A. Zulazmi *et al.*, Zerumbone Alleviates Neuropathic Pain through the Involvement of l-Arginine-Nitric Oxide-cGMP-K⍰ ATP Channel Pathways in Chronic Constriction Injury in Mice Model. *Molecules* **22**, (2017).

67. T. F. Tzeng, S. S. Liou, Y. C. Tzeng, I. M. Liu, Zerumbone, a Phytochemical of Subtropical Ginger, Protects against Hyperglycemia-Induced Retinal Damage in Experimental Diabetic Rats. *Nutrients* **8**, (2016).

68. K. Ohnishi, K. Irie, A. Murakami, In vitro covalent binding proteins of zerumbone, a chemopreventive food factor. *Biosci Biotechnol Biochem* **73**, 1905-1907 (2009).

69. G. Li Volti, P. Murabito, Pharmacologic induction of heme oxygenase-1: it is time to take it seriously*. *Crit Care Med* **42**, 1967-1968 (2014).

70. G. J. Zhao *et al.*, Contributions of Nrf2 to Puerarin Prevention of Cardiac Hypertrophy and its Metabolic Enzymes Expression in Rats. *J Pharmacol Exp Ther* **366**, 458-469 (2018).

71. C. Park *et al.*, Protective Effect of Phloroglucinol on Oxidative Stress-Induced DNA Damage and Apoptosis through Activation of the Nrf2/HO-1 Signaling Pathway in HaCaT Human Keratinocytes. *Mar Drugs* **17**, (2019).

72. M. Zhao *et al.*, 5-aminolevulinic acid combined with sodium ferrous citrate ameliorates H2O2-induced cardiomyocyte hypertrophy via activation of the MAPK/Nrf2/HO-1 pathway. *Am J Physiol Cell Physiol* **308**, C665-672 (2015).

73. J. Tongers *et al.*, Heme oxygenase-1 inhibition of MAP kinases, calcineurin/NFAT signaling, and hypertrophy in cardiac myocytes. *Cardiovasc Res* **63**, 545-552 (2004).

74. Z. Wang, S. O. Ka, Y. Lee, B. H. Park, E. J. Bae, Butein induction of HO-1 by p38 MAPK/Nrf2 pathway in adipocytes attenuates high-fat diet induced adipose hypertrophy in mice. *Eur J Pharmacol* **799**, 201-210 (2017).

75. K. R. Brunt *et al.*, Heme oxygenase-1 inhibits pro-oxidant induced hypertrophy in HL-1 cardiomyocytes. *Exp Biol Med (Maywood)* **234**, 582-594 (2009).

76. A. Zhang, M. Wang, P. Zhuo, Unc-51 like autophagy activating kinase 1 accelerates angiotensin II-induced cardiac hypertrophy through promoting oxidative stress regulated by Nrf-2/HO-1 pathway. *Biochem Biophys Res Commun* **509**, 32-39 (2019).

77. J. Huang *et al.*, Harmine is an effective therapeutic small molecule for the treatment of cardiac hypertrophy. *Acta Pharmacol Sin*, (2021).

78. X. Lian *et al.*, Robust cardiomyocyte differentiation from human pluripotent stem cells via temporal modulation of canonical Wnt signaling. *Proc Natl Acad Sci U S A***109**, E1848-1857 (2012).

Figures

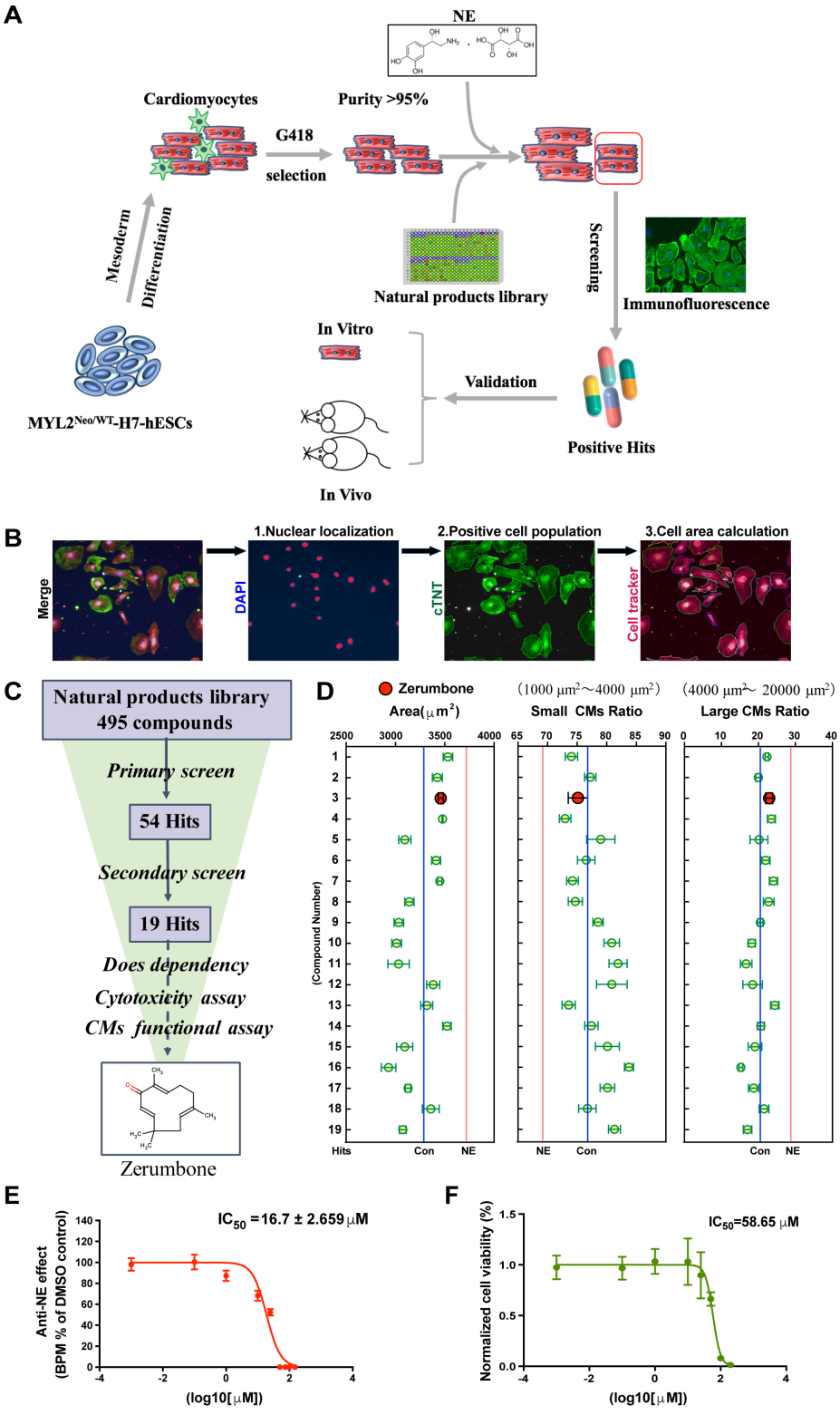

Figure 1

High-throughput screening for a library of small molecule natural compounds in NE-induced hypertrophy of hESC-CMs resulted in the identification of zerumbone. A, Schematic outline of the experimental procedures. **B,** A schematic overview of high-content analysis for CMs recognition and cell area calculation. Immunofluorescence images of cTnT (green) staining were used for identifying positive cells and Cell Tracker (deep red) for calculating cell area. All images were acquired and analyzed by high-

content imaging system after drug treatment for 5 days. **C,** The workflow demonstrating the screening strategy for identification of zerumbone. All compounds were tested in 4 duplicates at 10 μM. **D,** Ranked cell area, small CMs ratio, and large CMs ratio in NE-treated purified hESC-CMs exposed to 19 positive compounds after secondary screening. Red lines and blue lines indicate the baseline of hESC-CMs treated with and without NE (20μM), respectively. **E,** Dose-response curves of the anti-NE effect of zerumbone on beating frequency in hESC-CMs. **F,** Dose-response curves of hESC-CMs viability upon zerumbone treatment. Solid lines represent the best fits for calculating IC_{50} values (four-parameter dose-response curve). Mean ± SEM (n=3 biological replicates).

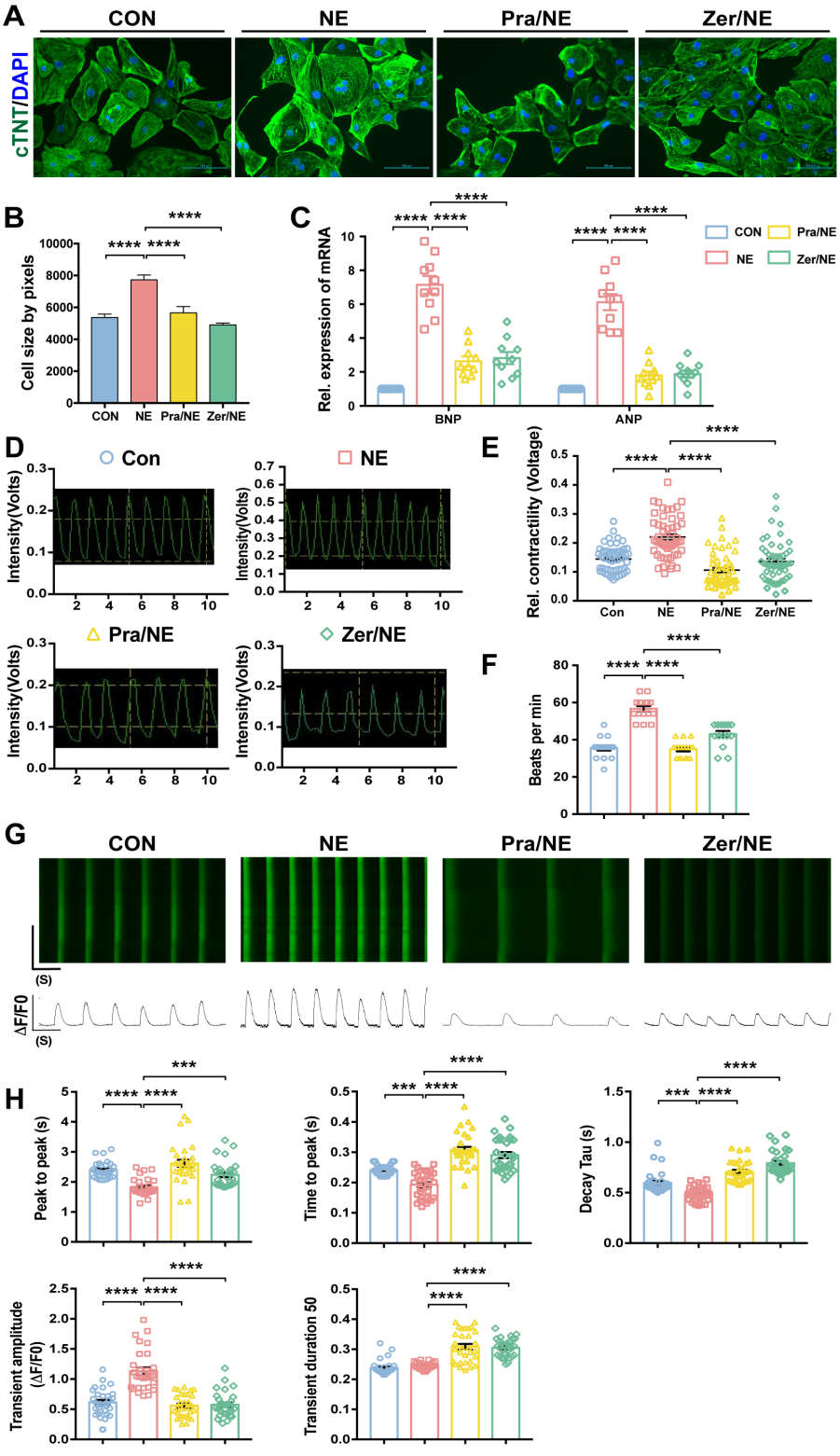

Figure 2

Zerumbone prevented NE-induced hypertrophy of hESC-CMs. A, Immunofluorescence images of cTnT-stained cardiomyocytes (green) after 5 days treatment. Scale bar: 100 μm. **B,** Quantification of cell area shown in A (n>400, measured from different visual fields of 3 independent experiments). **C,** qPCR analysis of *BNP* and *ANP* mRNA levels in CMs treated with NE, prazosin, or zerumbone as indicated (n=10). All data were normalized to β-actin expression. **D,** Representative images showing the contraction

traces of single CMs. **E-F,** Quantification of relative contractility (n=53) and beating frequency (n=16) of CMs following 24h compound treatment as indicated. **G,** Representative line scan images measuring calcium transients of single CMs after compound treatment for 24h. **H,** Quantification of calcium imaging parameters for each group (n=30). CMs were pretreated with prazosin (20 μM) or zerumbone (15 μM) for 3h and then stimulated with NE (20 μM). Values represent mean ± SEM of independent triplicate experiments. ***P*<0.01, ****P*<0.001, *****P*<0.0001 by one-way ANOVA.

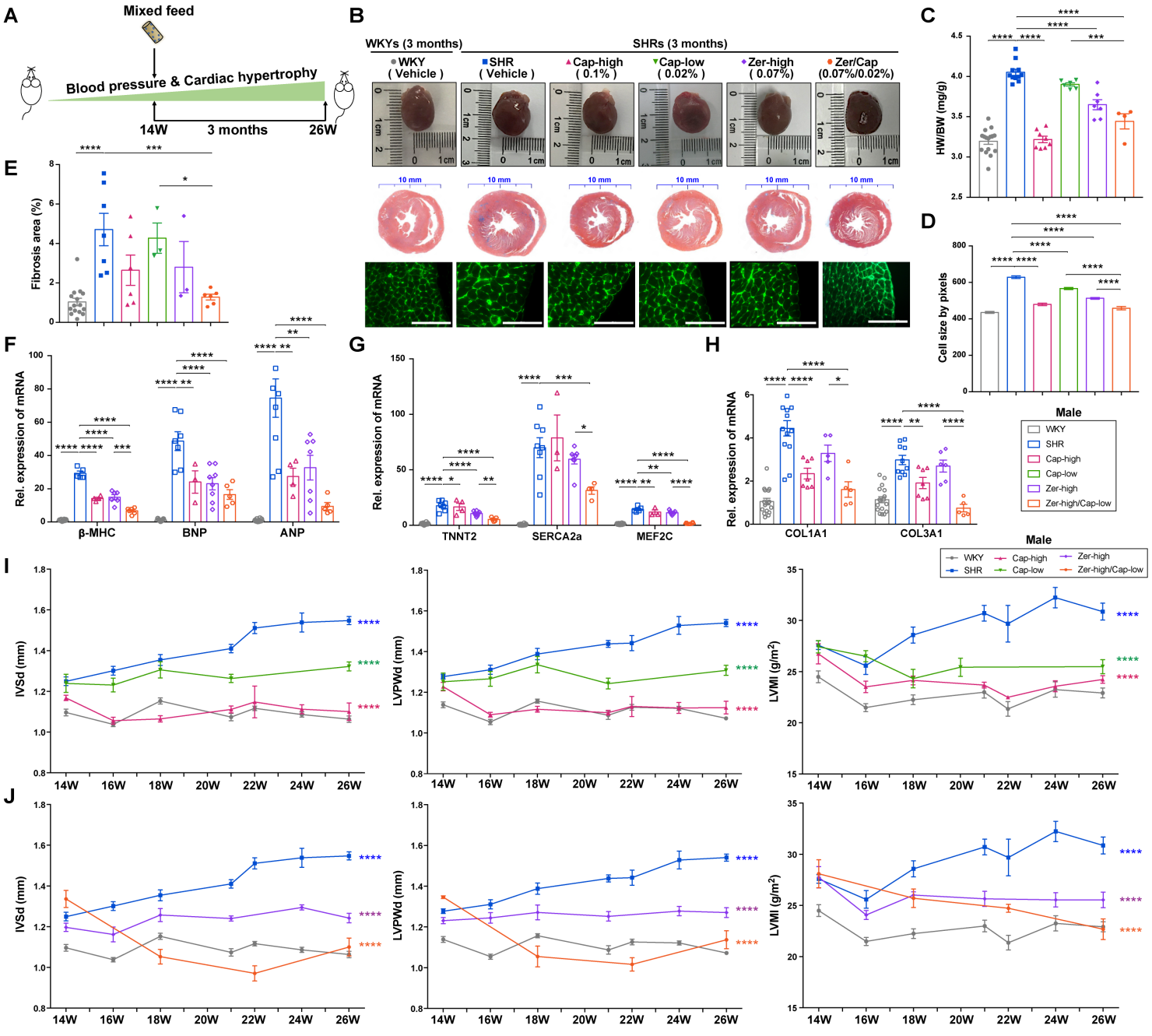

Figure 3

Zerumbone attenuates cardiac hypertrophy and remodeling in aged SHRs. A, Schematic diagram illustrating the therapeutic treatment strategy of zerumbone in aged SHRs that have developed cardiac hypertrophy. **B,** Representative images of gross heart morphology (top), Masson trichrome staining (middle), and WGA staining of heart tissues (bottom, scale bar: 100 μm). **C,** Heart weight to body weight ratios measured 3 months after treatment (n=16 for WKY; n=10 for SHR; n=8 for Cap-high; n=5 for Cap-low; n=7 for Zer-high; n=4 for Zer-high/Cap-low). **D,** Quantitative analysis of cardiomyocytes cross-sectional area with WGA staining (n>500, measured from different visual fields of 3 samples per group). **E,** Quantification of the ratio of cardiac fibrosis area with Masson trichrome staining (n=15 for WKY; n=7 for SHR; n=6 for Cap-high; n=3 for Cap-low; n=3 for Zer-high; n=6 for Zer-high/Cap-low). **F-H,** qPCR analysis showing mRNA levels of hypertrophic genes in heart (*β-MHC*, *BNP*, *ANP*, *TNNT2*, *SERCA2a*, *MEF2C*, *COL1A1*, *COL3A1*, normalized to *18S* expression, n>9 for WKY; n>5 for SHR; n>3 for Cap-high; n>5 for Zer-high; n>4 for Zer-high/Cap-low). **I-J,** Echocardiographic analysis of interventricular septum (IVSd), left ventricular posterior wall thickness at diastole (LVPWd), and left ventricular mass index (LVMI) after captopril or/and zerumbone treatment (SHR *vs.*WKY at 26W, others *vs.*SHR at 26W, by one-way ANOVA). For more detailed cardiac functional data, please refer to Supplementary Table 4. All data represent mean ± SEM; one-way ANOVA. **P*<0.05, ***P*<0.01, ****P*<0.001, *****P*<0.0001.

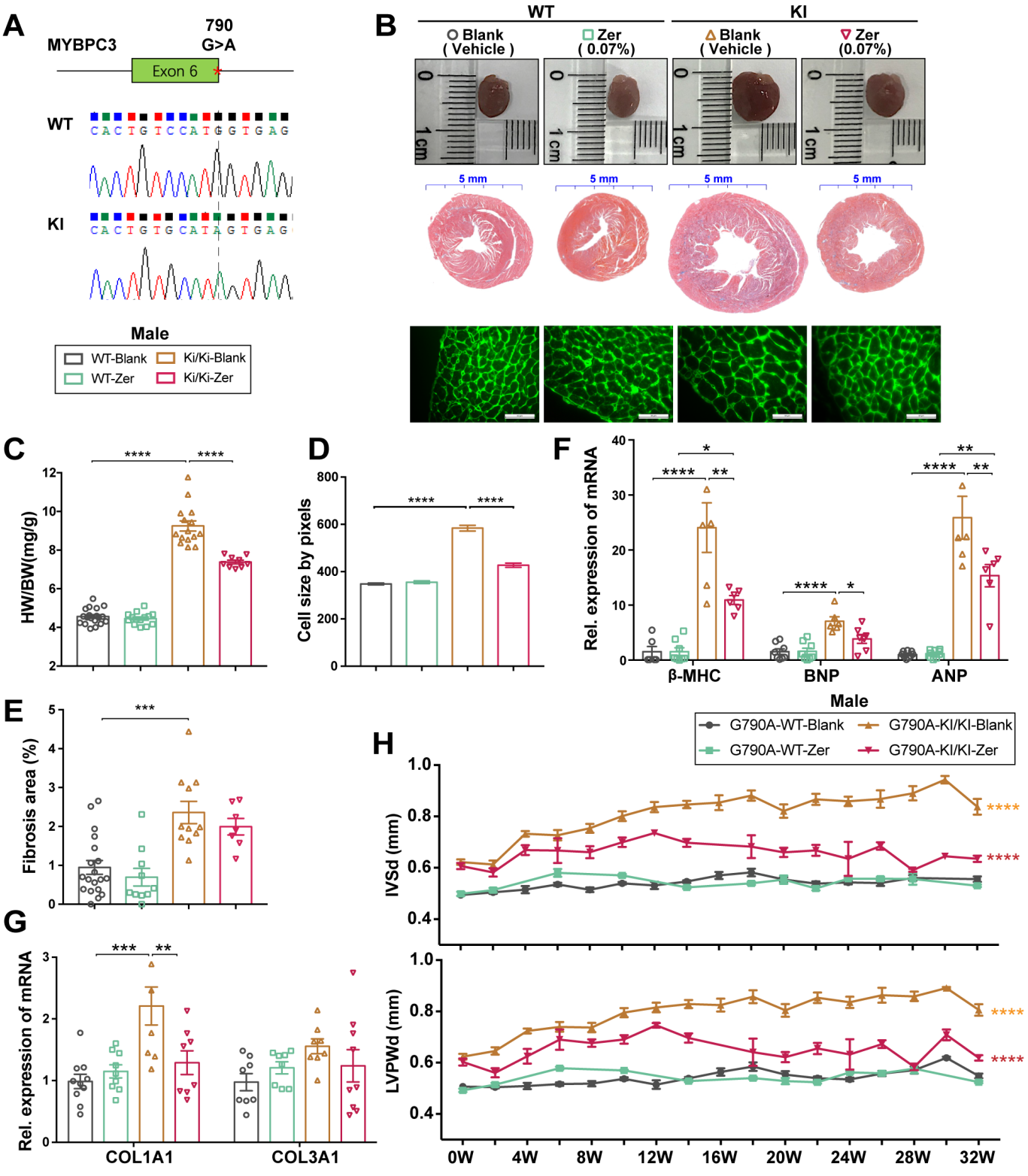

Figure 4

Zerumbone repressed cardiac hypertrophy in HCM mice. A, Schematic diagram depicting the sequence of the cMyBP-C G790A knock-in mouse carrying the point mutation on the last nucleotide of exon 6 (G>A). **B,** Representative images of isolated gross heart morphology (top), Masson trichrome staining (middle), and WGA staining of heart tissues (bottom, scale bar: 50 μm). **C,** Heart weight to body weight ratio of each group (n=19 for WT-Blank; n=14 for WT-Zer; n=15 for KI/KI-Blank; n=9 for KI/KI-Zer). **D,** Quantification of

CMs cross-sectional area with WGA staining (n>450, measured from different visual fields of 3 samples per group). **E,** Quantification of the ratio of cardiac fibrosis area with Masson trichrome staining (n=19 for WT-Blank; n=10 for WT-Zer; n=11 for KI/KI-Blank; n=7 for KI/KI-Zer). **F-G,** qPCR analysis of mRNA levels of hypertrophic genes in heart (*β-MHC*, *BNP*, *ANP*, *TNNT2*, *SERCA2a*, *MEF2C*, *COL1A1*, *COL3A1*, normalized to *18S* expression, n>6 for WT-Blank; n>8 for WT-Zer; n>6 for KI/KI-Blank; n>6 for KI/KI-Zer). **H,** Echocardiographic analysis of interventricular septum (IVSd) and left ventricular posterior wall values (LVPWd) at diastole after zerumbone treatment (KI/KI-Blank *vs.* WT-Blank at 32W, KI/KI-Zer *vs.* KI/KI-Blank at 32W, by one-way ANOVA). For more detailed cardiac functional data, please refer to Supplementary Table 6. All data represent mean ± SEM; one-way ANOVA. **P*<0.05, ***P*<0.01, ****P*<0.001, *****P*<0.0001.

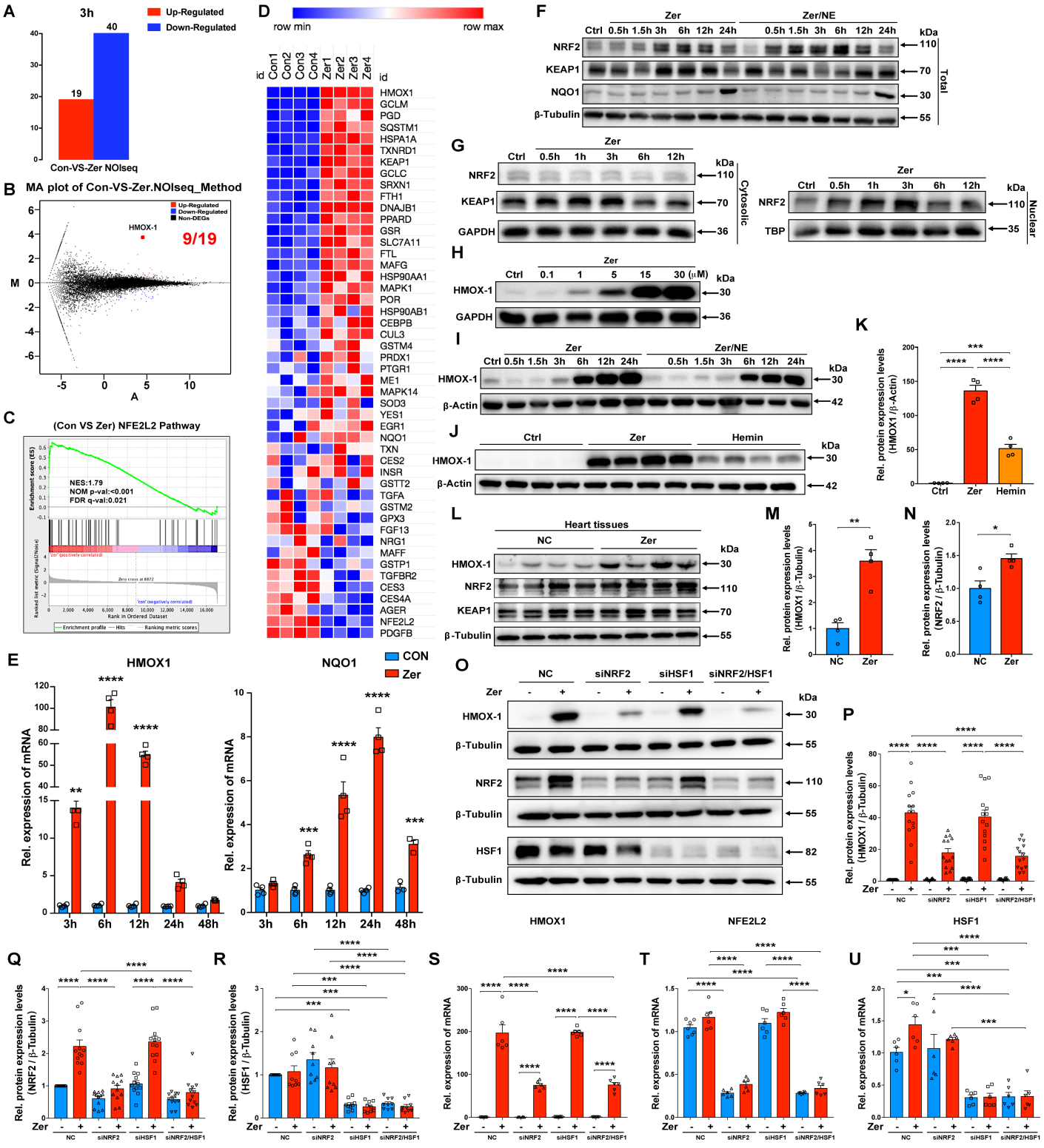

Figure 5

Zerumbone activates NRF2 signaling with a highly efficient induction of HO-1. A, Quantification of up- and down-regulated genes from RNAseq data in hESC-CMs treated with 15 μM zerumbone for 3h. **B,** A volcano plot showing the significantly up-regulated (red) and down-regulated (blue) genes. 9 of 19 upregulated genes belong to the NRF2 downstream target genes. **C,** Gene set enrichment analysis (GSEA) showing the enrichment of NRF2 target gene set from hESC-CMs treated with zerumbone for 3h (n=4

replicates). **D,** Heat map indicating the differentially expressed genes from NRF2 target gene set in hESC-CMs. **E,** Relative *HMOX1* and *NQO1* mRNA levels in hESC-CMs treated with 15 μM zerumbone for indicated time periods; n=3-4 replicates, by two-way ANOVA. **F,** Immunoblotting of KEAP1, NRF2 and NQO1 in total lysates from hESC-CMs treated with zerumbone (15 μM) only or zerumbone (15 μM)/NE (20 μM) for indicated time point. **G,** The protein expression of NRF2 in the cytoplasm and nuclei, and KEAP1 expression in the cytoplasm. **H-I,** HMOX1 protein expression in hESC-CMs treated with indicated concentrations of zerumbone for 12h (top) or 15 μM zerumbone for the above-stated time periods (bottom). **J-K,** Western blot analysis of HMOX1 protein levels in hESC-CMs after treated with 15 μM zerumbone or hemin for 12h; n=4 replicates, one-way ANOVA. **L-N,** Immunoblotting analysis of HMOX1, NRF2, and KEAP1 in heart tissues of C57 mice after given zerumbone (70 mg/kg) by intragastric administration for 24h; n=4 mice/group, two-tailed Student's t test. **O,** Western blot of HMOX1, NRF2 and HSF1 from hESC-CMs transfected with NRF2 or/and HSF1 siRNA for 72h followed by 12h zerumbone (15 μM) treatment. **P-R,** Quantification of relative protein expression of HMOX-1 (n=14 replicates), NRF2 (n=12 replicates) and HSF1 (n=9 replicates) in hESC-CMs treated with or without zerumbone after interference. **S-U,** The mRNA expression of *HMOX-1*, *NFE2L2* and *HSF1* in hESC-CMs followed by 72h siRNA interference and 6h zerumbone (15 μM) treatment (n=6 replicates); one-way ANOVA. Data represent mean ± SEM of biologically independent experiments. *P<0.05, **P<0.01, ***P<0.001, ****P<0.0001.

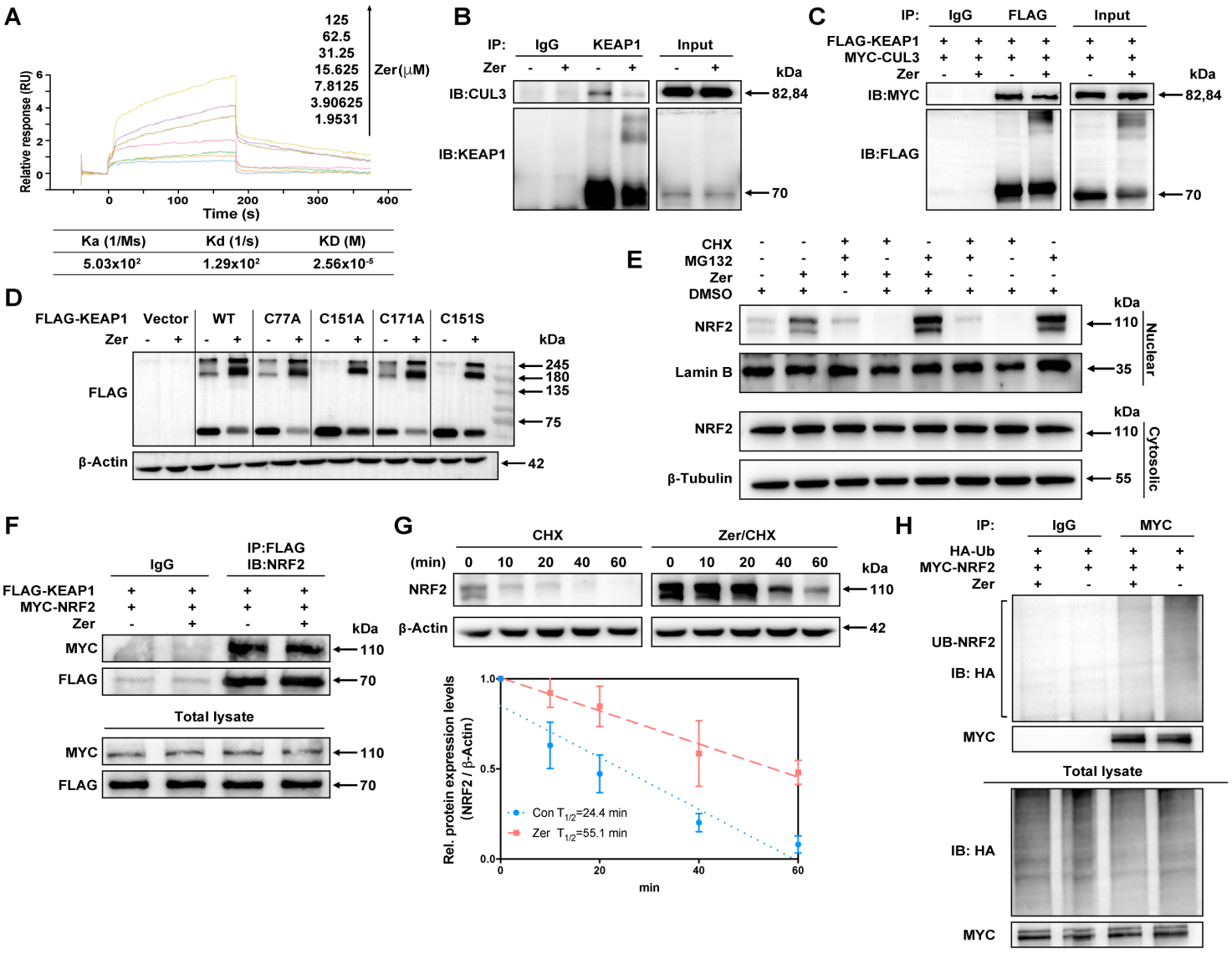

Figure 6

Zerumbone triggers a formation of HMW KEAP1 and activates NRF2 signaling pathway through CUL3-dependent inhibition of ubiquitination. A, SPR analysis showing the direct binding of zerumbone to KEAP1 with a KD of 25.6 μM. RU, response unit. **B,** Immunoprecipitation analysis of interaction between endogenous CUL3 and KEAP1 protein in hESC-CMs. Cell lysates were harvested from hESC-CMs treated with zerumbone (30 μM) for 4h. **C,** Immunoprecipitation analysis of interaction between exogenous overexpressed CUL3 and KEAP1 protein in HEK293T. HEK293T cells transfected with FLAG-KEAP1 and MYC-CUL3 plasmids (36h) were treated with 30 μM zerumbone for 4h. **D,** Anti-Flag western blot analysis of cell lysates from HEK293T expressing WT-FLAG-KEAP1 or cysteine-mutant FLAG-KEAP1(C77A, C151A, C151S, C171A) treated with DMSO or 15μM zerumbone. HEK293T cells were transfected with indicated plasmids for 24h and then treated with zerumbone for 6h. **E,** NRF2 protein levels from hESC-CMs in nuclei and cytoplasm treated with different combination of zerumbone (15 μM), CHX (20 μg/ml), and MG132 (10 μM) for 1h. **F,** Immunoprecipitation analysis of the effect of zerumbone on the in *vitro* interaction between NRF2 and KEAP1. Cell lysates from HEK293T cells transfected with FLAG-KEAP1 and MYC-

NRF2 plasmids for 36h were incubated with zerumbone (100 μM) for 3h at 4°C before antibody (anti-FLAG) addition. **G,** Immunoblotting analysis of NRF2 protein half-life ($T_{1/2}$). Total lysates from hESC-CMs pretreated with zerumbone (30 μM) for 3h and then cotreated with CHX (20 μg/ml) were harvested at indicated time points, n=3 independent experiments. **H,** Immunoprecipitation analysis of NRF2 ubiquitination. HEK293T cells were co-transfected to express MYC-NRF2 and HA-Ub for 36h and then treated with zerumbone (30 μM) along with MG132 (10 μM) for 4h. Data represent mean ± SEM.

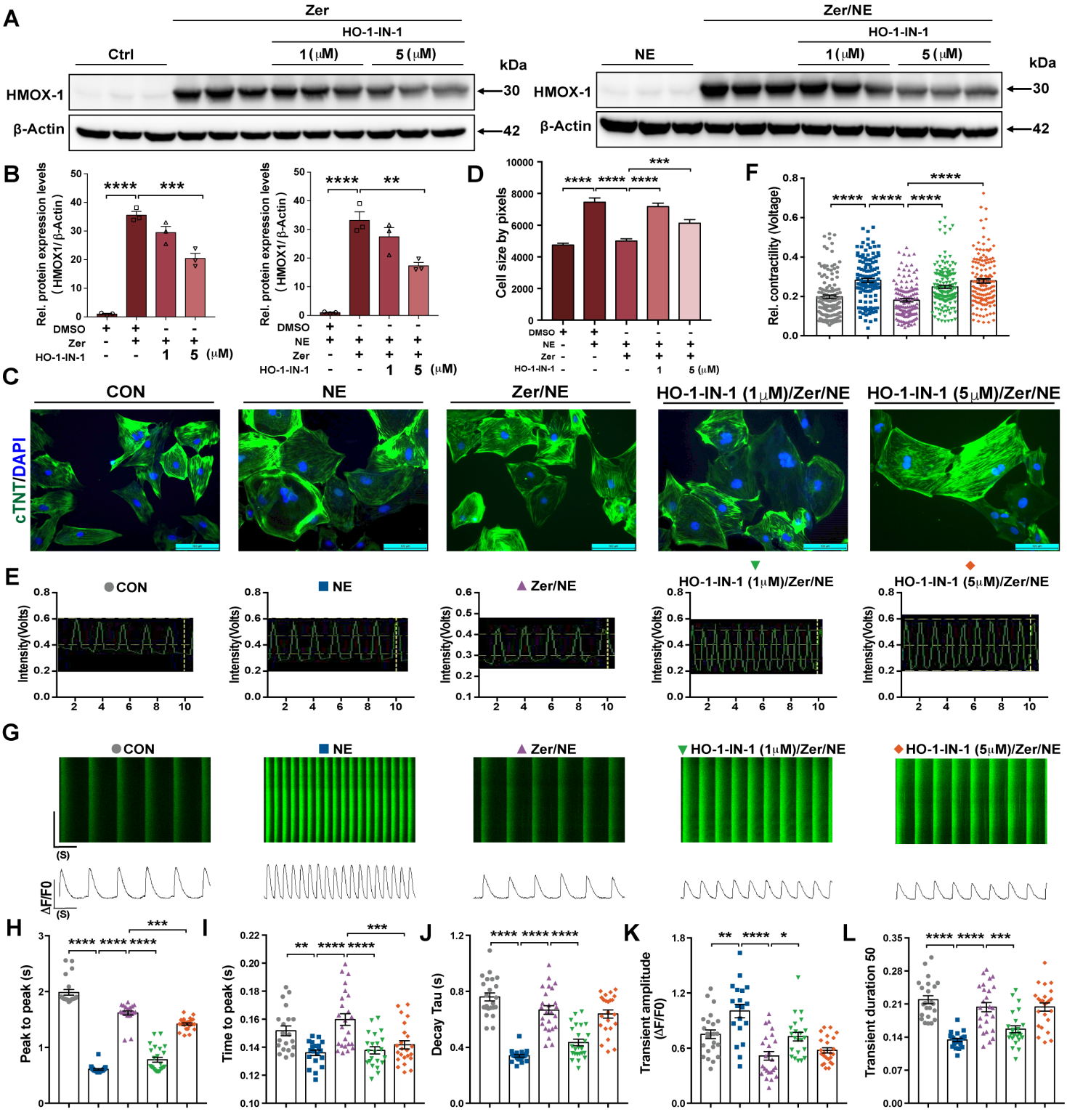

Figure 7

Downregulation of HO-1 blunts the cardioprotective effect of zerumbone in cardiac hypertrophy. A-B, Representative western blotting and quantification of the changes in HMOX1 protein level in hESC-CMs treated with HO-1-IN-1 (an inhibitor of HMOX1) as indicated concentrations for 12h (n=3 replicates). **C-D,** Representative immunofluorescence images of cTnT-stained cardiomyocytes (green) and quantification of cell size (n>300, measured from different visual fields of 3 independent experiments). Scale bar: 100

μm. Cardiomyocytes were treated under indicated conditions for 3 days after seeded on dishes for 2 days culture. **E-F,** Representative images showing the contraction traces of single cardiomyocytes and quantification of relative contractility of cardiomyocytes following 24h compound treatment as indicated (n>130). **G-L,** Representative line scan images measuring calcium transients of single cardiomyocytes after 24h treatment and quantification of calcium imaging parameters for each group (n>20). In HO-1-IN-1 treated group, hESC-CMs were pre-treated with HO-1-IN-1 for 0.5h before zerumbone (15 μM) only or zerumbone (15 μM)/NE (20 μM) addition. Values represent mean ± SEM; one-way ANOVA. *P<0.05, **P<0.01, ***P<0.001, ****P<0.0001.

Supplementary Files

This is a list of supplementary files associated with this preprint. Click to download.

- Supplementaryinformation.pdf